Micro-mechanics models for an imperfect interface under anti-plane shear load: hypersingular integral formulations

Xue Wang, Whye-Teong Ang* and Hui Fan
Division of Engineering Mechanics
School of Mechanical and Aerospace Engineering
Nanyang Technological University
Singapore 639798

Abstract

Two micro-mechanics models are proposed for an imperfect (weak) interface between two anisotropic elastic half-spaces under anti-plane shear load. The imperfect interface in the first model contains an array of periodically distributed micro-cracks with random lengths and positions. The second model, a simplified version of the first, is a three-phase model in which a period length of the interface contains a single representative micro-crack, perfectly bonded parts and an effective region. Both models are formulated in terms of hypersingular integral equations which may be solved by boundary element procedures to calculate the effective interface stiffness and the critical failure load of the interface.

This is the preprint of an article accepted for publication in *Engineering Analysis with Boundary Elements*. When the article is published, it can be accessed at: http://dx.doi.org/10.1016/j.enganabound.2012.07.005. *Status as at 23 July 2012.*

* Author for correspondence (W. T. Ang)
E-mail: mwtang@ntu.edu.sg
http://www.ntu.edu.sg/home/mwtang/

1 Introduction

A perfect bond between two joined materials is an idealization. In reality, microscopic imperfections or gaps are bound to be present along the interface of the materials. Thus, the analysis of imperfect interfaces in layered and composite materials is a subject of considerable interest among many researchers (see Andrianov *et al* [2], Avila-Pozos and Movchan [4], Fan and Wang [9], Torquato and Rintoul [12] and other references therein).

An interface weakened by micro-cracks may be macroscopically modeled as a continuously damaged interface. In the context of elasticity, the macroscopic model of such an imperfect weak interface may be described by the interfacial conditions in Benveniste and Miloh [5] which involve elastic displacement fields that are discontinuous across opposite sides of the interface. The interfacial displacement jump is linearly related to the traction on the interface, that is, the weak interface may be physically interpreted as a continuous distribution of springs.

A micro-mechanics problem of interest is to estimate the effective stiffness coefficients of the "springs" in the macroscopic model by taking into consideration the micro-cracks on the interface. Fan and Sze [10] proposed a three-phase model that may be used to investigate the problem for the case in which the imperfect interface is subject to an anti-plane deformation. The finite element method was employed in [10] to solve numerically the boundary value problem of the model.

For the purpose of estimating the effective interface stiffness of the anti-plane imperfect interface between two anisotropic elastic half-spaces, two micro-mechanics models of the interface are proposed in the current paper. In the first micro-mechanics model, a given region of the imperfect interface is modeled as containing an arbitrary number of arbitrarily located micro-cracks of different lengths. Those micro-cracks in the region are then periodically duplicated over the entire interface between the two half-spaces. The second model, which may be regarded as a simplified version of the first, is a three-phase model which follows quite closely the spirit of the work in Fan and Sze [10]. In the three-phase model here, the interface is periodic and a period length of the interface contains a single representative micro-crack, perfectly bonded parts and an effective region that is modeled as a continuously damaged interface with a yet to be determined interface stiffness.

The boundary value problems in both models are formulated in terms of hypersingular integral equations. The unknown function in the hyper-

singular integral equations is directly given by the jump in the anti-plane displacement across opposite sides of the micro-cracks or the effective regions. Once the hypersingular integral equations for the first micro-crack model are solved, the effective interface stiffness of the imperfect interface under anti-plane deformations can be easily calculated through an averaging formula. For the three-phase model, a predictor-corrector method that iterates to and fro between solving the hypersingular integral equations and calculating the unknown interface stiffness of the effective region are used to solve the boundary value problem. The hypersingular integral equations in both models are solved here by using boundary element procedures. The hypersingular integral approach for solving problems involving cracks and imperfect interfaces is well established in the literature (see, for example, Ang [3], Chen and Hong [7] and Hong and Chen [11]).

The mode III (anti-plane) stress intensity factors at the tips of the micro-cracks in the two micro-mechanics models mentioned above, which can be easily extracted from the solutions of the hypersingular integral equations, can be used to determine the critical load for the failure of the interface. The calculation of the critical load based on the those models is also considered in the current paper.

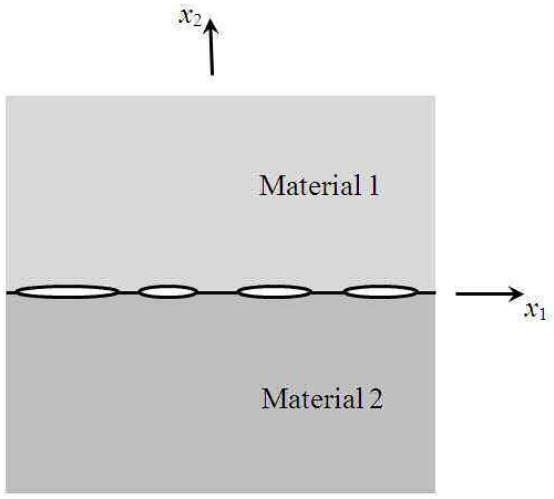

Figure 1. Micro-cracks and micro-voids distributed along the interface between two dissimilar elastic half-spaces.

2 Imperfect interface problems

With reference to a Cartesian coordinate system $Ox_1x_2x_3$, consider two dissimilar anisotropic elastic materials occupying the half-spaces $x_2 > 0$ and $x_2 < 0$. The half-spaces are imperfectly joined along the interface $x_2 = 0$, with micro-cracks and micro-voids distributed along the entire interface. Refer to Figure 1.

The bimaterial is assumed to undergo an anti-plane deformation such that the only non-zero component of the elastic displacement is along the x_3 direction and depends on only x_1 and x_2. According to Hooke's law, the anti-plane stress σ_{3j} is related to the anti-plane displacement u_3 by

$$\begin{aligned} \sigma_{31} &= C_{55}\frac{\partial u_3}{\partial x_1} + C_{45}\frac{\partial u_3}{\partial x_2}, \\ \sigma_{32} &= C_{45}\frac{\partial u_3}{\partial x_1} + C_{44}\frac{\partial u_3}{\partial x_2}, \end{aligned} \tag{1}$$

where C_{44}, C_{45} and C_{55} are independent elastic coefficients of the bimaterials defined by

$$(C_{44}, C_{45}, C_{55}) = \begin{cases} (C_{44}^{(1)}, C_{45}^{(1)}, C_{55}^{(1)}) & \text{for } x_2 > 0, \\ (C_{44}^{(2)}, C_{45}^{(2)}, C_{55}^{(2)}) & \text{for } x_2 < 0, \end{cases} \tag{2}$$

with $(C_{45}^{(p)})^2 - C_{44}^{(p)}C_{55}^{(p)} < 0$.

From (1) and the stress equilibrium equation, the anti-plane displacement u_3 has to satisfy the elliptic partial differential equation

$$C_{55}\frac{\partial^2 u_3}{\partial x_1^2} + 2C_{45}\frac{\partial^2 u_3}{\partial x_1 \partial x_2} + C_{44}\frac{\partial^2 u_3}{\partial x_2^2} = 0, \tag{3}$$

in the half-spaces $x_2 > 0$ and $x_2 < 0$.

Two specific problems on the mechanics of the imperfect interface between the anisotropic half-spaces are studied here.

Problem I. On the macroscopic level, the imperfect interface between the elastic materials in the half-spaces may be modeled as a continuous distribution of springs (see, for example, Hashin [13]). For anti-plane deformations,

the macroscopic model of the continuously damaged interface $x_2 = 0$ is given by the boundary conditions

$$\left.\begin{array}{r} \sigma_{32}(x_1, 0^+) = \sigma_{32}(x_1, 0^-) \\ k\Delta u_3(x_1) = \sigma_{32}(x_1, 0^+) \end{array}\right\} \text{ for } -\infty < x_1 < \infty, \tag{4}$$

where σ_{ij} are components of the elastic stress, $\Delta u_3(x_1) = u_3(x_1, 0^+) - u_3(x_1, 0^-)$ denotes the jump of u_3 across the interface, u_3 is the x_3 component of the elastic displacement and k is the interface stiffness. The problem is to estimate the effective k for the macroscopic model of the interface by taking into consideration some details of the micro-cracks.

Problem II. The imperfect interface starts to fail if the mode III stress intensity factor at any of the micro-crack tips exceeds a critical value $K_{III}^{\text{critical}}$ which depends on the composition of the bimaterial. If the far-field stress in the bimaterial is given by

$$\sigma_{3j}(x_1, x_2) \to \delta_{j2} S_0 \quad \text{as } x_1^2 + x_2^2 \to \infty, \tag{5}$$

the problem is to determine the critical constant anti-plane load S_0 needed to initiate the failure of the interface.

3 Micro-mechanics models

To study the two problems stated in Section 2 above, two micro-mechanics models of the imperfect interface are used here.

3.1 Multiple micro-crack model

In this model, a region of length L on the interface is modeled as containing M arbitrarily located micro-cracks of possibly different lengths. On the part of the interface defined by $0 < x_1 < L$, $x_2 = 0$, a typical m-th crack has tips $(a^{(m)}, 0)$ and $(b^{(m)}, 0)$, where $a^{(m)}$ and $b^{(m)}$ are constants such that

$$0 < a^{(1)} < b^{(1)} < a^{(2)} < b^{(2)} < \cdots < a^{(M)} < b^{(M)} < L.$$

Micro-cracks on the remaining parts of the interface are given by $a^{(m)} + nL < x_1 < b^{(m)} + nL$ for $m = 1, 2, \cdots, M$ and $n = \pm 1, \pm 2, \cdots$, that

is, the remaining micro-cracks are periodically distributed exact replicas of the M micro-cracks on $0 < x_1 < L$, $x_2 = 0$. For illustration, a sketch of the micro-cracks for $M = 3$ is given in Figure 2.

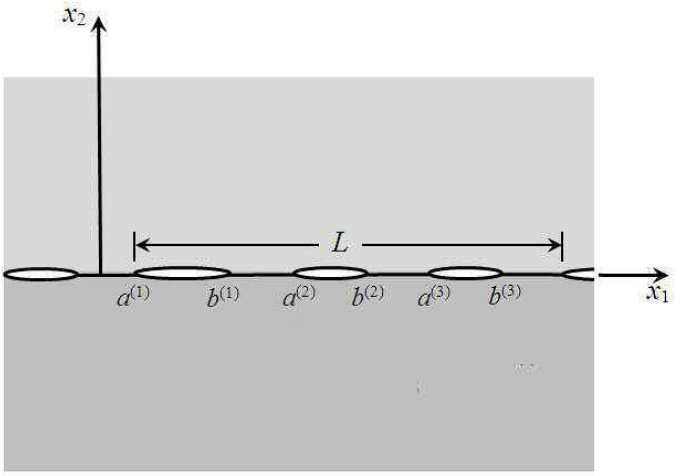

Figure 2. An illustrative sketch of the periodic micro-crack model for $M = 3$.

For the micro-crack model here, we define the fracture ratio parameter R by

$$R = \frac{\text{sum of lengths of the } M \text{ micro-cracks}}{L} = \frac{1}{L}\sum_{m=1}^{M}(b^{(m)} - a^{(m)}). \qquad (6)$$

The bimaterial is subject to an external anti-plane shear stress S_0 at infinity, the micro-cracks are traction free and the displacement u_3 and the stress σ_{32} are continuous across the uncracked parts of the interface $x_2 = 0$. Specifically, at the micro-level, the conditions on the interface are given by

$$\begin{aligned} \sigma_{32}(x_1, 0^+) &= \sigma_{32}(x_1, 0^-) = 0 \text{ for } a^{(m)} + pL < x_1 < b^{(m)} + pL \\ &\qquad (m = 1, 2, \cdots, M;\ p = 0, \pm 1, \pm 2, \cdots), \end{aligned} \qquad (7)$$

and

$$\left.\begin{aligned} u_3(x_1, 0^+) &= u_3(x_1, 0^-) \\ \sigma_{32}(x_1, 0^+) &= \sigma_{32}(x_1, 0^-) \end{aligned}\right\} \text{ on uncracked parts of the interface.} \qquad (8)$$

Note that (7) implies that the micro-cracks are traction free. To determine the jump in u_3 (that is, Δu_3) across opposite faces of the micro-cracks, the partial differential equation in (3) has to be solved subject to (7) and (8). The stress formula (A2) in the Appendix may be used to derive the hypersingular integral equations

$$\begin{aligned}
&\sum_{m=1}^{M} \oint\!\!\!\!\!\!= \int_{a^{(m)}}^{b^{(m)}} \Delta u_3(x_1)[\frac{1}{(x_1-\xi_1)^2} + \frac{1}{(L+x_1-\xi_1)^2} \\
&+\frac{1}{(L+\xi_1-x_1)^2} + \frac{1}{L^2}\psi^*(\frac{L+x_1-\xi_1}{L}) + \frac{1}{L^2}\psi^*(\frac{L+\xi_1-x_1}{L})]dx_1 \\
= \quad & -\frac{\pi(\beta^{(1)}+\beta^{(2)})}{\beta^{(1)}\beta^{(2)}} S_0 \text{ for } a^{(n)} < \xi_1 < b^{(n)} \ (n = 1, 2, \cdots, M).
\end{aligned} \tag{9}$$

where $\oint\!\!\!\!\!\!=$ denotes that the integral is to be interpreted in the Hadamard finite-part sense, $\psi^*(x)$ is related to the trigamma function $\psi_1(x)$ as explained in the Appendix and $\beta^{(p)}$ is defined by

$$\beta^{(p)} = \sqrt{|[C_{45}^{(p)}]^2 - C_{44}^{(p)} C_{55}^{(p)}|}. \tag{10}$$

Once Δu_3 is determined for each of the micro-cracks by solving the hypersingular integral equations in (9), the effective interface stiffness k for the macroscopic model of the imperfect interface may be estimated by an averaging the jump in u_3 over the micro-cracks.

The micro-mechanics model described above may be used with samples of a large number of micro-cracks with random lengths and randomly chosen positions along a period length of the interface to carry out statistical simulations of the imperfect interface.

3.2 Three-phase model

The micro-crack model above may be simplified to a so called three-phase model. The interface is still periodic in the simplified model, but a period length of the interface, as denoted by $0 < x_1 < L$, $x_2 = 0$, which is assumed to contain many micro-cracks, is modeled as comprising three parts as follows:

(a) a single representative micro-crack $c^{(1)} < x_1 < d^{(1)}$, $x_2 = 0$,

(b) perfectly bonded parts defined by $0 < x_1 < c^{(1)}$ and $d^{(1)} < x_1 < c^{(2)}$ on $x_2 = 0$, and

(c) a so called effective region $c^{(2)} < x_1 < d^{(2)}$, $x_2 = 0$, where the constants $c^{(1)}$, $c^{(2)}$, $d^{(1)}$ and $d^{(2)}$ are such that $0 < c^{(1)} < d^{(1)} < c^{(2)} < d^{(2)} = L$, $c^{(1)} = c^{(2)} - d^{(1)}$ and $c^{(2)}$ is very much smaller than L.

The micro-crack, the perfectly bonded parts and the effective region are periodically reproduced with period L to the left and right along the x_1 axis. Refer to Figure 3.

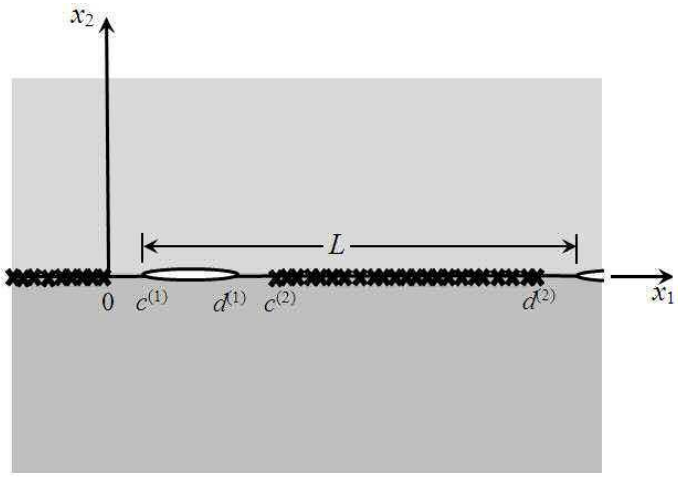

Figure 3. A sketch of the three-phase micro-model of the imperfect interface.

For the simplified model here, the fracture ratio parameter R which to corresponds to (6) is defined by

$$R = \frac{d^{(1)} - c^{(1)}}{c^{(2)}}. \tag{11}$$

As in the micro-crack model, the micro-cracks here are traction free and the conditions on the uncracked parts given by (8). The conditions on the effective regions are the ones in the macroscopic model of the imperfect interface, that is,

$$\left.\begin{array}{l} \sigma_{32}(x_1, 0^+) = \sigma_{32}(x_1, 0^-) \\ \\ k\Delta u_3(x_1) = \sigma_{32}(x_1, 0^+) \end{array}\right\} \text{ for } c^{(2)} + pL \;<\; x_1 < d^{(2)} + pL$$

$$(p \;=\; 0, \pm 1, \pm 2, \cdots), \tag{12}$$

but the interface stiffness k here is an unknown to be determined as part of the solution.

For the three-phase model here, the stress formula (A2) in the Appendix may be used to derive the hypersingular integral equations

$$\begin{aligned}
&\sum_{i=1}^{2} \neq\!\!\!\!\!\!\int_{c^{(i)}}^{d^{(i)}} \Delta u_3(x_1)[\frac{1}{(x_1-\xi_1)^2}+\frac{1}{(d^{(2)}+x_1-\xi_1)^2} \\
&+\frac{1}{(d^{(2)}+\xi_1-x_1)^2}+\frac{1}{[d^{(2)}]^2}\psi^*(\frac{d^{(2)}+x_1-\xi_1}{d^{(2)}}) \\
&+\frac{1}{[d^{(2)}]^2}\psi^*(\frac{d^{(2)}+\xi_1-x_1}{d^{(2)}})]dx_1 \\
= \; &-\frac{\pi(\beta^{(1)}+\beta^{(2)})}{\beta^{(1)}\beta^{(2)}} \begin{cases} S_0 & \text{for } c^{(1)}<\xi_1<d^{(1)}, \\ S_0-k\Delta u_3(\xi_1) & \text{for } c^{(2)}<\xi_1<d^{(2)}, \end{cases}
\end{aligned} \tag{13}$$

where Δu_3 denotes the discontinuity of u_3 across opposite faces of the micro-cracks and the effective regions.

As the interface stiffness k is a macroscopic quantity that is not known a priori, the hypersingular integral equations in (13) are to be solved together with

$$\frac{k}{c^{(2)}} \int_{c^{(1)}}^{d^{(1)}} \Delta u_3(x_1)dx_1 = S_0 \tag{14}$$

for the unknowns k and $\Delta u_3(x_1)$ for $c^{(1)}<x_1<d^{(1)}$ and $c^{(2)}<x_1<d^{(2)}$. Note that (14) is derived from the relation

$$k \times (\text{average value of } \Delta u_3(x_1) \text{ over } 0<x_1<c^{(2)}) \; = S_0.$$

4 Estimation of the effective interface stiffness

In this section, the two micro-mechanics models are used to solve Problem I, that is, to estimate the effective interface stiffness k for the macroscopic model of the interface. The hypersingular integral equations in (9) and (14) are solved using boundary element procedures.

4.1 Statistical simulation approach

In this approach, the hypersingular integral equations in (9) (for the multiple micro-crack model) are solved for large samples of a selected number of randomly chosen micro-cracks randomly located within one period length L of the interface $x_2 = 0$. For a given sample of micro-cracks, once $\Delta u_3(x_1)$ is determined for $a^{(m)} < x_1 < b^{(m)}$ $(m = 1, 2, \cdots, M)$, the interface stiffness k of the imperfect interface $x_2 = 0$ can then be computed using the averaging formula

$$k = S_0 L[\sum_{m=1}^{M} \int_{a^{(m)}}^{b^{(m)}} \Delta u_3(x_1) dx_1]^{-1}. \tag{15}$$

The mean value of k with its standard deviation can then be calculated from all the samples of micro-cracks.

For the numerical solution of (9), the crack $a^{(n)} < x_1 < b^{(n)}$, $x_2 = 0$, is discretized into $N^{(n)}$ elements. The elements are intervals on the x_1 axis given by $[x^{(m)}, y^{(m)}]$ for $m = 1, 2, \cdots, (N^{(1)} + N^{(2)} + ... + N^{(n)})$, that is,

$$\left.\begin{aligned} x^{(j)} &= \frac{a^{(1)} + b^{(1)}}{2} - \frac{b^{(1)} - a^{(1)}}{2} \cos(\frac{[j-1]\pi}{N^{(1)}}) \\ y^{(j)} &= \frac{a^{(1)} + b^{(1)}}{2} - \frac{b^{(1)} - a^{(1)}}{2} \cos(\frac{j\pi}{N^{(1)}}) \end{aligned}\right\} \text{ for } j = 1, 2, \cdots, N^{(1)},$$

$$\left.\begin{aligned} x^{(N^{(1)}+N^{(2)}+\cdots+N^{(n-1)}+j)} &= \frac{a^{(n)} + b^{(n)}}{2} - \frac{b^{(n)} - a^{(n)}}{2} \cos(\frac{[j-1]\pi}{N^{(n)}}) \\ y^{(N^{(1)}+N^{(2)}+\cdots+N^{(n-1)}+j)} &= \frac{a^{(n)} + b^{(n)}}{2} - \frac{b^{(n)} - a^{(n)}}{2} \cos(\frac{j\pi}{N^{(n)}}) \end{aligned}\right\}$$
$$\text{for } j = 1, 2, \cdots, N^{(n)} \text{ and } n = 2, 3, \cdots, M. \tag{16}$$

Note that (16) distributes more elements of shorter lengths nearer to the tips of the micro-cracks.

The displacement jump function $\Delta u_3(x_1)$ is written in the form

$$\begin{aligned} \frac{\beta^{(1)}\beta^{(2)}}{S_0(\beta^{(1)} + \beta^{(2)})} \Delta u_3(x_1) &= \sqrt{(x_1 - a^{(n)})(b^{(n)} - x_1)}\, w(x_1) \\ \text{for } a^{(n)} &\le x_1 \le b^{(n)} \ (n = 1, 2, \cdots, M), \end{aligned} \tag{17}$$

where $w(x_1)$ is approximated as a constant over an element, that is,

$$w(x_1) \simeq w^{(m)} \text{ (constant) for } x_1 \in [x^{(m)}, y^{(m)}], \tag{18}$$

With the above approximations, the hypersingular integral equations in (9) can be collocated at $\xi_1 = \xi^{(j)}$ ($\xi^{(j)}$ is the midpoint of the j-th element $[x^{(j)}, y^{(j)}]$) ($j = 1, 2, \cdots, N^{(1)} + N^{(2)} + ... + N^{(M)}$) to obtain the system of linear algebraic equations

$$\begin{aligned}
&\sum_{m=1}^{N^{(1)}+N^{(2)}+...+N^{(M)}} w^{(m)}[F(y^{(m)}, \xi^{(j)}, s^{(m)}, t^{(m)}) - F(x^{(m)}, \xi^{(j)}, s^{(m)}, t^{(m)}) \\
&+F(y^{(m)}, \xi^{(j)} - L, s^{(m)}, t^{(m)}) - F(x^{(m)}, \xi^{(j)} - L, s^{(m)}, t^{(m)}) \\
&+F(y^{(m)}, \xi^{(j)} + L, s^{(m)}, t^{(m)}) - F(x^{(m)}, \xi^{(j)} + L, s^{(m)}, t^{(m)}) \\
&+\frac{1}{L^2}\{\psi^*(\frac{L + \xi^{(m)} - \xi^{(j)}}{L}) + \psi^*(\frac{L + \xi^{(j)} - \xi^{(m)}}{L})\} \\
&\times(K(y^{(m)}, s^{(m)}, t^{(m)}) - K(x^{(m)}, s^{(m)}, t^{(m)}))] \\
= \; &-\pi \text{ for } j = 1, 2, \cdots, N^{(1)} + N^{(2)} + ... + N^{(M)},
\end{aligned} \tag{19}$$

where

$$\left.\begin{array}{rcl} s^{(m)} & = & a^{(p)} \\ t^{(m)} & = & b^{(p)} \end{array}\right\} \text{ if } [x^{(m)}, y^{(m)}] \text{ lies on } a^{(p)} < x_1 < b^{(p)},\ x_2 = 0,$$

$$\begin{aligned}
F(x, \xi, a, b) &= F_0(x, \xi, a, b) + F_1(x, \xi, a, b), \\
K(x, a, b) &= -\frac{1}{4}(-2x + a + b)\sqrt{(b - x)(x - a)} \\
&\quad +\frac{1}{8}(a - b)^2 \arctan(\frac{2x - a - b}{2\sqrt{(b - x)(x - a)}}),
\end{aligned}$$

$$\begin{aligned}
F_0(x, \xi, a, b) &= -\frac{((x - a)(b - x))^{3/2}}{(\xi - a)(b - \xi)(x - \xi)} + \frac{(a + b - \xi - x)\sqrt{(x - a)(b - x)}}{(\xi - a)(b - \xi)} \\
&\quad -\begin{cases} \arctan(\dfrac{2x - a - b}{2\sqrt{(x - a)(b - x)}}) & \text{for} \quad (x - a)(b - x) \neq 0, \\ \operatorname{sgn}(2x - a - b)\dfrac{\pi}{2} & \text{for} \quad (x - a)(b - x) = 0, \end{cases}
\end{aligned}$$

$$
\begin{aligned}
& F_1(x,\xi,a,b) \\
= \; & \frac{(a+b-2\xi)}{4\sqrt{(b-\xi)\,(\xi-a)}}\{\,\ln|2\sqrt{(b-\xi)\,(\xi-a)}\sqrt{(x-a)(b-x)} \\
& \qquad -(\xi a+\xi b-2x\xi-2ab+ax+bx)| \\
& \quad -\ln|2\sqrt{(b-\xi)\,(\xi-a)}\sqrt{(x-a)(b-x)} \\
& \qquad +(\xi a+\xi b-2x\xi-2ab+ax+bx)|\,\} \\
& \qquad \text{if } \; (b-\xi)\,(\xi-a)>0,
\end{aligned}
$$

$$
\begin{aligned}
F_1(x,\xi,a,b) \; = \; & -\frac{(a+b-2\xi)}{2\sqrt{(\xi-b)\,(\xi-a)}} \\
& \times \begin{cases} \arctan(-\dfrac{(\xi a+\xi b-2x\xi-2ab+ax+bx)}{2\sqrt{(\xi-b)\,(\xi-a)}\sqrt{(x-a)(b-x)}}) \\ \qquad \text{for} \;\; (x-a)(b-x)\neq 0, \\ \mathrm{sgn}(-(\xi a+\xi b-2x\xi-2ab+ax+bx))\dfrac{\pi}{2} \\ \qquad \text{for} \;\; (x-a)(b-x)=0, \end{cases} \\
& \text{if } \; (b-\xi)\,(\xi-a)<0. \qquad (20)
\end{aligned}
$$

Once the system of linear algebraic equations is solved for $w^{(m)}$, the interface stiffness k of the imperfect interface can be computed using

$$
\begin{aligned}
& \frac{(\beta^{(1)}+\beta^{(2)})}{\beta^{(1)}\beta^{(2)}}k \\
= \; & L\,\{\sum_{m=1}^{N^{(1)}+N^{(2)}+\ldots+N^{(M)}} w^{(m)}[K(y^{(m)},s^{(m)},t^{(m)})-K(x^{(m)},s^{(m)},t^{(m)})]\}^{-1}. \qquad (21)
\end{aligned}
$$

4.2 Three-phase model

Equations (13) and (14) in the three-phase model may be solved numerically for the interface stiffness k and the displacement jump Δu_3 across opposite micro-crack faces by using the following boundary element procedure.

We discretize the micro-crack $c^{(1)} < x_1 < d^{(1)}$, $x_2 = 0$ into $N^{(1)}$ boundary elements given by the intervals $[x^{(1)}, y^{(1)}]$, $[x^{(2)}, y^{(2)}]$, $\cdots$, $[x^{(N^{(1)}-1)}, y^{(N^{(1)}-1)}]$ and $[x^{(N^{(1)})}, y^{(N^{(1)})}]$ and the effective region $c^{(2)} < x_1 < d^{(2)}$, $x_2 = 0$ into

$N^{(2)}$ boundary elements given by $[x^{(N^{(1)}+1)}, y^{(N^{(1)}+1)}]$, $[x^{(N^{(1)}+2)}, y^{(N^{(1)}+2)}]$, $\cdots$, $[x^{(N^{(1)}+N^{(2)}-1)}, y^{(N^{(1)}+N^{(2)}-1)}]$ and $[x^{(N^{(1)}+N^{(2)})}, y^{(N^{(1)}+N^{(2)})}]$, where

$$\left.\begin{aligned} x^{(j)} &= \frac{c^{(1)}+d^{(1)}}{2} - \frac{d^{(1)}-c^{(1)}}{2}\cos(\frac{[j-1]\pi}{N^{(1)}}) \\ y^{(j)} &= \frac{c^{(1)}+d^{(1)}}{2} - \frac{d^{(1)}-c^{(1)}}{2}\cos(\frac{j\pi}{N^{(1)}}) \end{aligned}\right\} \text{for } j = 1, 2, \cdots, N^{(1)},$$

$$\left.\begin{aligned} x^{(N^{(1)}+j)} &= \frac{c^{(2)}+d^{(2)}}{2} - \frac{d^{(2)}-c^{(2)}}{2}\cos(\frac{[j-1]\pi}{N^{(2)}}) \\ y^{(N^{(1)}+j)} &= \frac{c^{(2)}+d^{(2)}}{2} - \frac{d^{(2)}-c^{(2)}}{2}\cos(\frac{j\pi}{N^{(2)}}) \end{aligned}\right\} \text{for } j = 1, 2, \cdots, N^{(2)}. \tag{22}$$

Note that (22) distributes more elements of shorter lengths nearer to the tips of the micro-crack and the effective region.

We let

$$\begin{aligned} &\frac{\beta^{(1)}\beta^{(2)}}{S_0(\beta^{(1)}+\beta^{(2)})}\Delta u_3(x_1) \\ &= \begin{cases} \sqrt{(x_1-c^{(1)})(d^{(1)}-x_1)}w(x_1) & \text{for } c^{(1)} < x_1 < d^{(1)}, \\ w(x_1) & \text{for } c^{(2)} < x_1 < d^{(2)}, \end{cases} \end{aligned} \tag{23}$$

where the function $w(x_1)$ is approximated as a constant over each of the elements, that is,

$$w(x_1) \simeq w^{(n)} \text{ (constant) for } x_1 \in [x^{(n)}, y^{(n)}]$$

$$(n = 1, 2, \cdots, N^{(1)} + N^{(2)}). \tag{24}$$

Using (23) and (24), we collocate (13) at $\xi_1 = \xi^{(n)}$ (where $\xi^{(n)}$ is the midpoint of the n-th element $[x^{(n)}, y^{(n)}]$) to obtain the algebraic equations

$$
\begin{aligned}
&\sum_{m=1}^{N^{(1)}} w^{(m)}[F(y^{(m)},\xi^{(n)},c^{(1)},d^{(1)})-F(x^{(m)},\xi^{(n)},c^{(1)},d^{(1)})\\
&+F(y^{(m)},\xi^{(n)}-d^{(2)},c^{(1)},d^{(1)})-F(x^{(m)},\xi^{(n)}-d^{(2)},c^{(1)},d^{(1)})\\
&+F(y^{(m)},\xi^{(n)}+d^{(2)},c^{(1)},d^{(1)})-F(x^{(m)},\xi^{(n)}+d^{(2)},c^{(1)},d^{(1)})\\
&+\frac{1}{[d^{(2)}]^2}\{\psi^*(\frac{d^{(2)}+\xi^{(m)}-\xi^{(n)}}{d^{(2)}})+\psi^*(\frac{d^{(2)}+\xi^{(n)}-\xi^{(m)}}{d^{(2)}})\}\\
&\times(K(y^{(m)},c^{(1)},d^{(1)})-K(x^{(m)},c^{(1)},d^{(1)}))]\\
&+\sum_{m=1}^{N^{(2)}} w^{(N^{(1)}+m)}[G(x^{(N^{(1)}+m)},y^{(N^{(1)}+m)},\xi^{(n)})\\
&+G(x^{(N^{(1)}+m)},y^{(N^{(1)}+m)},\xi^{(n)}-d^{(2)})\\
&+G(x^{(N^{(1)}+m)},y^{(N^{(1)}+m)},\xi^{(n)}+d^{(2)})-\frac{(\beta^{(1)}+\beta^{(2)})\pi}{\beta^{(1)}\beta^{(2)}}kg^{((N^{(1)}+m)n)}\\
&+\frac{(y^{(N^{(1)}+m)}-x^{(N^{(1)}+m)})}{[d^{(2)}]^2}\{\psi^*(\frac{d^{(2)}+\xi^{(N^{(1)}+m)}-\xi^{(n)}}{d^{(2)}})\\
&+\psi^*(\frac{d^{(2)}+\xi^{(n)}-\xi^{(N^{(1)}+m)}}{d^{(2)}})\}\ ]\\
=\ & -\pi \text{ for } n=1,2,\cdots,N^{(1)}+N^{(2)},
\end{aligned}
\tag{25}
$$

where

$$
\begin{aligned}
G(x,y,\xi) &= \frac{y-x}{(\xi-x)(\xi-y)},\\
g^{(pk)} &= \begin{cases} 1 & \text{if } p=k\geq N^{(1)}+1,\\ 0 & \text{otherwise.}\end{cases}
\end{aligned}
\tag{26}
$$

With the above approximations, (14) can be written as

$$
\frac{(\beta^{(1)}+\beta^{(2)})}{\beta^{(1)}\beta^{(2)}}k=c^{(2)}\ \{\sum_{m=1}^{N^{(1)}} w^{(m)}[K(y^{(m)},c^{(1)},d^{(1)})-K(x^{(m)},c^{(1)},d^{(1)})]\}^{-1}.
\tag{27}
$$

The iterative procedure for solving (25) and (27) is outlined step by step below.

1. Give k an estimated value. For a cold start, k can be taken to be zero. Go to step 2.

2. For the current value of k, solve (25) for $w^{(m)}$ ($m = 1, 2, \cdots, N^{(1)} + N^{(2)}$). Go to step 3.

3. Use the current values of $w^{(m)}$ ($m = 1, 2, \cdots, N^{(1)}$) to calculate k according to (27). Check the absolute difference between the last two consecutive values of k. If the absolute difference agrees to a chosen number of significant figures, stop the iterative procedure. If the absolute difference does not satisfy the stopping criterion yet, go to step 2.

5 Failure analysis of imperfect interface

The micro-mechanics models are used here to determine the critical anti-plane load S_0 for initiating the failure of the imperfect interface.

5.1 Statistical simulation approach

For the micro-cracks in the multiple micro-crack model in Subsection 3.1, we define the mode III crack tip stress intensity factors

$$\left.\begin{array}{l} K_{III}^{(m)} = \lim\limits_{\varepsilon \to 0^+} \sqrt{2\varepsilon}\ \sigma_{32}(a^{(m)} - \varepsilon, 0) \\ K_{III}^{(M+m)} = \lim\limits_{\varepsilon \to 0^+} \sqrt{2\varepsilon}\sigma_{32}(b^{(m)} + \varepsilon, 0) \end{array}\right\} \text{ for } m = 1, 2, \cdots, M. \tag{28}$$

If the loading S_0 is such that

$$\max_{n=1,2,\cdots,2M} \{|K_{III}^{(n)}|\} > K_{III}^{\text{critical}}, \tag{29}$$

where $K_{III}^{\text{critical}}$ is the critical stress intensity factor of the bimaterial, then the imperfect interface starts to fail.

From (28), use of the stress formula (A2) in the Appendix gives

$$\begin{aligned} K_{III}^{(m)} &= \frac{S_0\sqrt{2(b^{(m)} - a^{(m)})}w(a^{(m)})}{2}, \\ K_{III}^{(M+m)} &= \frac{S_0\sqrt{2(b^{(m)} - a^{(m)})}w(b^{(m)})}{2}. \end{aligned} \tag{30}$$

Thus, once $w(x_1)$ is determined by solving numerically the hypersingular integral equations in (9) as described above, we can estimate $w(a^{(m)})$ and $w(b^{(m)})$to compute $K_{III}^{(m)}$ and $K_{III}^{(M+m)}$ approximately for $m = 1, 2, \cdots, M$.

From (29), if the magnitude of the mode III stress intensity factor is largest at the crack tip $(a^{(p)}, 0)$ then the critical load S_0^{critical} for the failure of the imperfect interface is given by

$$S_0^{\text{critical}} = \frac{2K_{III}^{\text{critical}}}{\sqrt{2(b^{(p)} - a^{(p)})}\,|w(a^{(p)})|}. \tag{31}$$

If the magnitude of the mode III stress intensity factor is maximum at the crack tip $(b^{(p)}, 0)$ then

$$S_0^{\text{critical}} = \frac{2K_{III}^{\text{critical}}}{\sqrt{2(b^{(p)} - a^{(p)})}\,|w(b^{(p)})|}. \tag{32}$$

In the statistical simulation approach, the hypersingular integral equations in (9) are solved for many samples of a selected number of randomly chosen micro-cracks randomly located within one period length L of the interface $x_2 = 0$. For each sample of micro-cracks, the critical load S_0^{critical} is calculated according to (31) or (32). The mean value of S_0^{critical} with its standard deviation can then be calculated from all the samples of micro-cracks.

5.2 Three-phase model

For the three-phase model in Subsection 3.2, the mode III stress intensity factors of the micro-crack $c^{(1)} < x_1 < d^{(1)}$, $x_2 = 0$ are defined by

$$\begin{aligned} K_{III}^{-} &= \lim_{\varepsilon \to 0^+} \sqrt{2\varepsilon}\ \sigma_{32}(c^{(1)} - \varepsilon, 0), \\ K_{III}^{+} &= \lim_{\varepsilon \to 0^+} \sqrt{2\varepsilon}\sigma_{32}(d^{(1)} + \varepsilon, 0). \end{aligned} \tag{33}$$

It follows that

$$\begin{aligned} K_{III}^{-} &= \frac{S_0\sqrt{2(d^{(1)} - c^{(1)})}w(c^{(1)})}{2}, \\ K_{III}^{+} &= \frac{S_0\sqrt{2(d^{(1)} - c^{(1)})}w(d^{(1)})}{2}. \end{aligned} \tag{34}$$

The critical load S_0^{critical} is given by

$$\begin{aligned} S_0^{\text{critical}} &= \frac{2K_{III}^{\text{critical}}}{\sqrt{2(d^{(1)}-c^{(1)})}\,|w(c^{(1)})|} \\ &= \frac{2K_{III}^{\text{critical}}}{\sqrt{2(d^{(1)}-c^{(1)})}\,|w(d^{(1)})|} \end{aligned} \tag{35}$$

By the symmetry of the three-phase model with constant load S_0, note that $K_{III}^- = K_{III}^+$.

Note that once $w(x_1)$ is determined by solving numerically the hypersingular integral equations in (9) the stress intensity factors K_{III}^- and K_{III}^+ and the critical load S_0^{critical} can be calculated using the formulae in (34) and (35).

6 Results and discussions

6.1 Verification of hypersingular integral formulations

For the fracture ratio parameter R not too close to 1,values of the effective interface stiffness k and the critical load S_0^{critical} predicted by the three-phase model in Subsection 3.2 are expected to be close to those predicted by the multiple micro-crack model in Subsection 3.1, if all the micro-cracks in the latter model are chosen to be of equal length and are evenly distributed on the interface. Thus, to verify that the hypersingular integral equations for the two models are correctly derived, we distribute evenly 15 micro-cracks, each of length $2a$, on one period length of the interface, calculate k and S_0^{critical} by solving the hypersingular integral equations in (9) and using (15) (multiple micro-crack model), and compare the values obtained with those calculated by solving the hypersingular integral equations (13) together with (14) (three-phase model).

For the comparison, plots of the non-dimensionalized interface stiffness $a(\beta^{(1)}+\beta^{(2)})k/(2\beta^{(1)}\beta^{(2)})$ and critical load $\sqrt{a}S_0^{\text{critical}}/K_{III}^{\text{critical}}$ against R for $0.10 < R < 0.90$ are given in Figures 4 and 5 respectively. The plots of the two models here are in good agreement, especially for smaller R. The percentage difference between the plots for $a(\beta^{(1)}+\beta^{(2)})k/(2\beta^{(1)}\beta^{(2)})$ ranges approximately from 0.25% ($R = 0.10$) to 2.5% ($R = 0.90$) and that for $\sqrt{a}S_0^{\text{critical}}/K_{III}^{\text{critical}}$ from 0.02% ($R = 0.10$) to 5.5% ($R = 0.90$). Thus, as expected, the multiple micro-crack model with evenly distributed equal length

micro-cracks gives values of k and S_0^{critical} that agree closely with those calculated using the three-phase model, provided that R is not too close to 1.

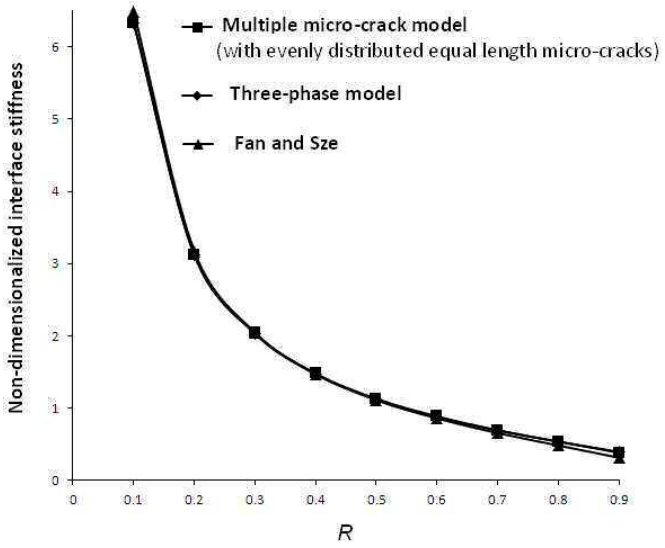

Figure 4. Plots of $a(\beta^{(1)} + \beta^{(2)})k/(2\beta^{(1)}\beta^{(2)})$ against R.

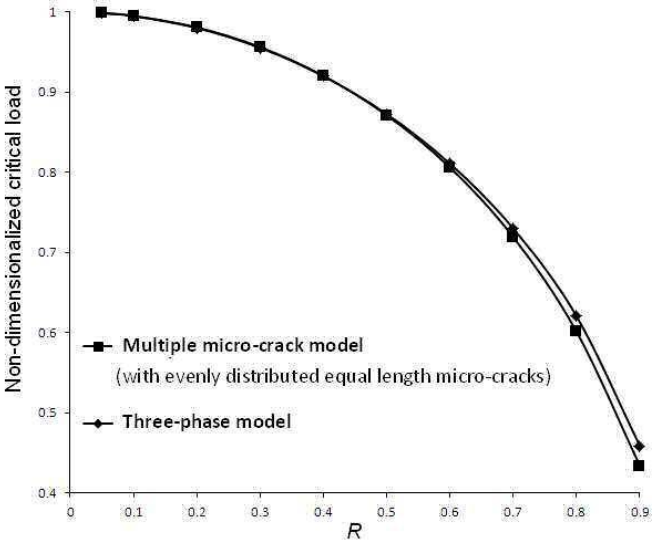

Figure 5. Plots of $\sqrt{a}S_0^{\text{critical}}/K_{III}^{\text{critical}}$ against R.

In Figure 4, $a(\beta^{(1)}+\beta^{(2)})k/(2\beta^{(1)}\beta^{(2)})$ computed using the finite element method three-phase model in Fan and Sze [10] is also plotted against R. It may be of interest to note that as many as ten thousand elements are employed in the finite element calculation for the three-phase model in [10], whereas less than three hundred elements are needed in the hypersingular boundary element calculation here for the three-phase model. The plots of $a(\beta^{(1)}+\beta^{(2)})k/(2\beta^{(1)}\beta^{(2)})$ calculated using the two models here and that of Fan and Sze [10] are nearly visually indistinguishable for smaller R, but the percentage difference between the value calculated using the multiple micro-crack model and that given in [10] ranges from 2.5% ($R = 0.10$) to 25% ($R = 0.90$). The percentage differences in the values of $a(\beta^{(1)}+\beta^{(2)})k/(2\beta^{(1)}\beta^{(2)})$ computed using the multiple micro-crack model and the three-phase model presented in this paper are roughly ten times smaller in magnitude, ranging from around 0.25% to 2.5% (as mentioned above). It is obvious that the multiple micro-crack model is in better agreement with the three-phase model here than with the one in [10]. This is because the three-phase model in Fan and Sze [10] ignores the effect that the stress induced by the micro-crack has on the effective region, that is, the model imposes the condition $k\Delta u_3(x_1) = S_0$ on the effective region (instead of $k\Delta u_3(x_1) = \sigma_{32}(x_1, 0^+)$ as done in (12) for the three-phase model here). Thus, it is not surprising that, compared to the three-phase model here, the three-phase model in [10] deviates much more significantly from the multiple micro-crack model if R is very to close to unity, that is, if there is a stronger interaction between the micro-crack and the effective region in the three-phase models.

6.2 Statistical simulations using multiple micro-crack model and comparisons with three-phase model

For statistical simulations, we take 15 micro-cracks to form a sample. The length of a micro-crack in the sample is normally distributed with a given theoretical mean and standard deviation. Once the lengths of the 15 micro-cracks are chosen randomly, the micro-cracks are randomly positioned within one period length L of the interface $x_2 = 0$, with the help of a pseudo-random number generator. If $\overline{a}$ denotes the average half length of the 15 micro-cracks, we take the length L to be $30\overline{a}/R$. For a chosen R, we solve (19) to calculate the non-dimensionalized interface stiffness $\overline{a}(\beta^{(1)}+\beta^{(2)})k/(2\beta^{(1)}\beta^{(2)})$ and critical load $\sqrt{\ell}\, S_0^{\text{critical}}/K_{III}^{\text{critical}}$,where ℓ is the half length of the micro-

crack that gives the maximum magnitude of the mode III crack tip stress intensity factor. We repeat the calculations using 50 different samples of 15 micro-cracks having the same theoretical mean and standard deviation of the micro-crack length. The average interface stiffness and the average critical load together with the corresponding standard deviations are then computed from the sample data of size 50.

Table 1. The percentage difference (% diff) and the number of standard deviations (no. of SD) between the average interface stiffness and the corresponding value predicted by the three-phase model for different values of the fracture ratio parameter R and theoretical standard deviation of the micro-crack length (SD of ML).

SD of ML	=	$0.05a$								
R	0.05	0.10	0.20	0.30	0.40	0.50	0.60	0.70	0.80	0.90
% diff	1.58	3.18	5.19	5.83	7.63	8.54	8.96	9.62	14.3	16.9
No. of SD	1.20	1.92	2.26	1.85	2.07	2.31	2.02	2.60	3.12	3.64
SD of ML	=	$0.10a$								
R	0.05	0.10	0.20	0.30	0.40	0.50	0.60	0.70	0.80	0.90
% diff	1.46	2.84	5.05	7.10	7.44	8.75	8.59	10.4	14.7	16.7
No. of SD	1.18	1.84	1.97	2.58	2.58	2.50	2.55	3.47	3.06	3.22
SD of ML	=	$1.50a$								
R	0.05	0.10	0.20	0.30	0.40	0.50	0.60	0.70	0.80	0.90
% diff	23.1	25.3	26.9	26.3	25.9	27.3	27.7	29.5	30.0	30.4
No. of SD	3.88	3.36	4.15	4.01	3.65	4.22	3.98	4.30	4.76	5.31
SD of ML	=	$1.90a$								
R	0.05	0.10	0.20	0.30	0.40	0.50	0.60	0.70	0.80	0.90
% diff	27.3	27.9	29.9	28.8	29.8	27.0	29.6	30.3	29.4	31.6
No. of SD	3.22	4.04	4.09	3.58	3.97	3.84	4.95	3.90	4.46	6.67

We compare the average effective interface stiffness computed from the sample data of size 50 with the corresponding value predicted by the three-phase model in Subsection 3.1 by examining the percentage difference (% diff) and the number of standard deviations (no. of SD) between the two

values as defined by

$$\% \text{ diff} = \left| \frac{(\text{value from three-phase model}) - (\text{average value})}{(\text{value from three-phase model})} \right| \times 100\%,$$

$$\text{No. of SD} = \left| \frac{(\text{value from three-phase model}) - (\text{average value})}{(\text{standard deviation of the data from average value})} \right|.$$

Table 1 shows the values of the above percentage difference and the number of standard deviations for statistical simulations with the theoretical mean of the micro-crack length fixed at $2a$ (where a is a basic length) and selected values of the standard deviation of the micro-crack length (SD of ML).

For a fixed R, if the theoretical standard deviation of the micro-crack length is small compared with the theoretical mean of the micro-crack length, the percentage difference between the average interface stiffness and the corresponding value predicted by the three-phase model tends to be smaller. If the theoretical standard deviation is close to the theoretical mean, the number of standard deviations between the average interface stiffness and the value predicted by the three-phase model is 4 or greater, that is, the interface stiffness predicted by the three-phase model is not likely to be within the range of data collected from the statistical simulations, even if R is small. For the theoretical standard deviation given by $0.05a$ and $0.10a$, the number of standard deviations between the average interface stiffness and the value predicted by the three-phase model is less than 3, mainly around 2, for lower values of R. In all the simulations, the average value of the interface stiffness is found to be less than the corresponding value given by the three-phase model.

In Figure 6, the average non-dimensionalized stiffness from the statistical simulations with the theoretical mean and standard deviation of the micro-crack length given by $2a$ and $0.10a$ respectively is plotted against R and compared with the corresponding value predicted by the three-phase model. A similar comparison is made in Figure 7 for the average non-dimensionalized interface stiffness from the statistical simulations with the theoretical mean and standard deviation of the micro-crack length given by $2a$ and $1.50a$ respectively.

The difference between the two plots under comparison is more obvious in Figure 7 (with a larger standard deviation of the micro-crack length) than in Figure 6 (with a smaller standard deviation of the micro-crack length). Although the gap between the minimum and maximum values of the data for the non-dimensionalized interface stiffness from the statistical simulations and the difference in the two plots in each of the figures seems smaller for R closer to 1, the actual percentage difference between the average interface stiffness and the corresponding value predicted by the three-phase model may actually be bigger for larger R (as shown in Table 1).

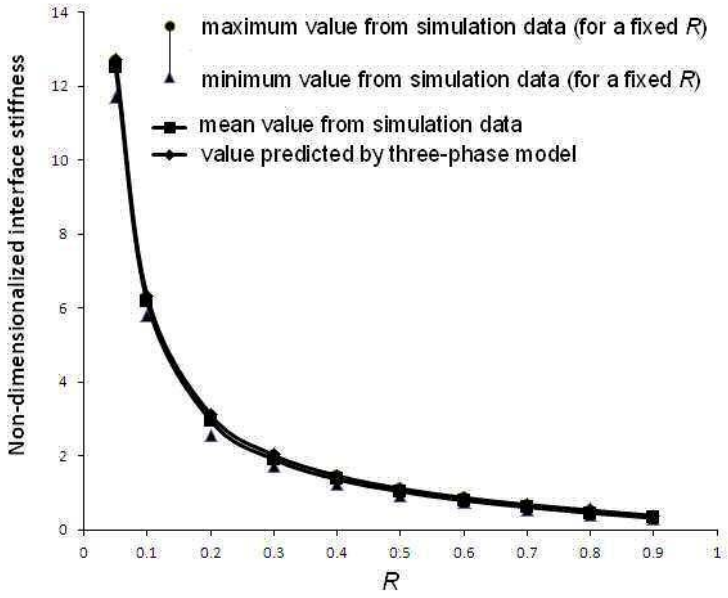

Figure 6. A comparison of the average interface stiffness from the statistical simulations (mean and standard deviation of the micro-crack length given by $2a$ and $0.10a$ respectively) with the corresponding value predicted by the three-phase model.

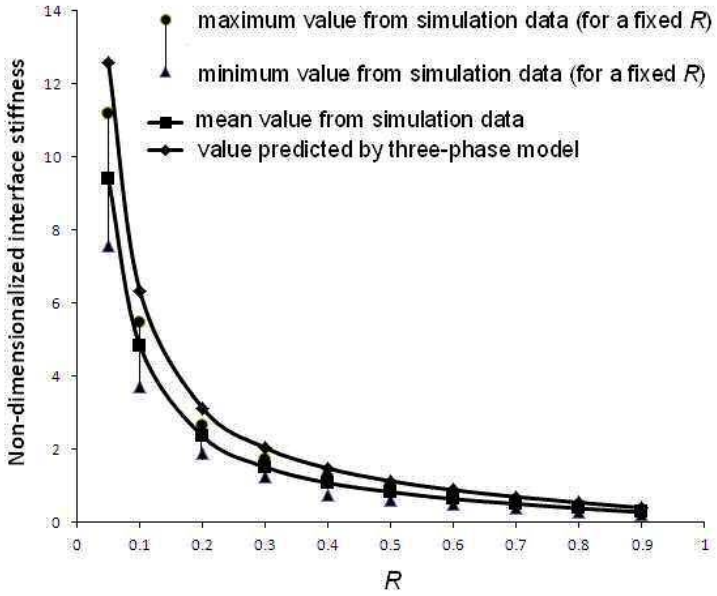

Figure 7. A comparison of the average interface stiffness from the statistical simulations (mean and standard deviation of the micro-crack length given by $2a$ and $1.50a$ respectively) with the corresponding value predicted by the three-phase model.

The average critical load (AVL) of $\sqrt{\ell}S_0^{\text{critical}}/K_{III}^{\text{critical}}$ (ℓ is the half length of the micro-crack that gives the maximum mode III crack tip stress intensity factor) and the minimum and the maximum non-dimensionalized critical load (min CL and max CL respectively) from the sample data of size 50 in the statistical simulations are given in Table 2 for the theoretical mean of the micro-crack length given by $2a$, several different values of the theoretical standard deviation of the micro-crack length and selected values of R. For a given R, the corresponding critical load given by the three-phase model (as plotted in Figure 5 against R) is closer to the maximum critical load than to the average and minimum critical load.There is a very significant difference between the minimum critical load and the critical load calculated using the three-phase model. Thus, the three-phase model cannot be relied upon to predict the failure of the imperfect interface. Table 2 shows that the critical load reduces significantly as R increases. This is expected as there is a stronger interaction between the micro-cracks for larger R (higher density of micro-cracks on the interface).

Table 2. The maximum, average and minimum values of the critical load $\sqrt{\ell}S_0^{\text{critical}}/K_{III}^{\text{critical}}$ (max CL, AVL and min CL respectively) from the sample data of size 50 in the statistical simulations with the theoretical mean of the micro-crack length given by $2a$ for several different values of the theoretical standard deviation of the micro-crack length (SD of ML) and selected values of R.

SD of ML	$= 0.05a$					
R	0.05	0.10	0.30	0.50	0.70	0.90
max CL	0.9987	0.9880	0.8768	0.7150	0.5963	0.3237
AVL	0.8897	0.8013	0.6656	0.4698	0.3345	0.1422
min CL	0.4655	0.4755	0.2856	0.1215	0.1062	0.0655
SD of ML	$= 0.10a$					
R	0.05	0.10	0.30	0.50	0.70	0.90
max CL	0.9997	0.9970	0.9153	0.7456	0.5639	0.2930
AVL	0.9176	0.8370	0.6150	0.4854	0.3367	0.1371
min CL	0.2356	0.4780	0.1448	0.2180	0.1240	0.0654
SD of ML	$= 1.50a$					
R	0.05	0.10	0.30	0.50	0.70	0.90
max CL	0.9997	0.9993	0.9917	0.8218	0.6597	0.3199
AVL	0.9471	0.8941	0.7329	0.5769	0.3622	0.1573
min CL	0.2993	0.4121	0.2756	0.1338	0.0723	0.0469
SD of ML	$= 1.90a$					
R	0.05	0.10	0.30	0.50	0.70	0.90
max CL	0.9997	0.9880	0.9690	0.9093	0.6967	0.3770
AVL	0.9662	0.9076	0.7346	0.6271	0.4129	0.1826
min CL	0.3784	0.3015	0.2857	0.1595	0.0955	0.0374

7 Summary and conclusion

Micro-mechanics models for an imperfect interface between two anisotropic elastic half-spaces under anti-plane shear load are proposed here. In the first model, which is the so called multiple micro-crack model, the imperfect interface contains an array of periodically distributed micro-cracks. The number of micro-cracks within a periodic length of the interface is arbitrary and so are their lengths and positions. The second model is a simplified three-phase model of the imperfect interface. In the simplified model, the

interface is still periodic but a period length of the interface is modeled as containing a single representative micro-crack, perfectly bonded parts and an effective region which may be regarded as continuously damaged spring-like interface with an unknown stiffness.

The multiple micro-crack model is a more general and realistic model as it takes into account not only the percentage of the interface damaged by micro-cracks but also the positions and the relative sizes of the micro-cracks present. Such details which are not captured in the three-phase model may play an important role in the macroscopic behaviours of the interface.

The hypersingular integral formulations for the models are verified by checking that they predict interface stiffness and the critical load for interface failure that are close to each other for the special case where the micro-cracks in the multiple micro-crack model have equal length, are evenly distributed and do not occupy a very large portion of the interface.

For more realistic cases of microscopically damaged interfaces, the multiple micro-crack model is used to carry out statistical simulations with randomly positioned micro-cracks whose lengths are normally distributed. Results from carrying out a large number of simulations seem to suggest the average value of the effective interface stiffness differs from the one predicted by the three-phase model by less than 10% if the percentage of the interface occupied by micro-cracks is 60% or less and the standard deviation of the micro-crack length is not greater than one tenth of the theoretical mean of the micro-crack length. It appears that the three-phase model may not be reliably used in general to predict the critical failure load if the interface has randomly positioned micro-cracks.

Acknowledgement. The authors would like to thank the anonymous reviewers for constructive comments and helpful suggestions which gave rise to the opportunity to revise and improve this paper.

References

[1] M. Abramowitz and I. Stegun, *Handbook of Mathematical Functions*, Dover, New York, 1970.

[2] I. V. Andrianov, V. I. Bolshakov, V. V. Danishevskyy and D. Weichert, Asymptotic study of imperfect interfaces in conduction through a gran-

ular composite material, *Proceedings of the Royal Society A* **466** (2010) 2707-2725.

[3] W. T. Ang, Elastodynamic antiplane deformation of a bimaterial with an imperfect viscoelastic interface: a dual reciprocity hypersingular boundary integral solution, *Applied Mathematical Modelling* **31** (2007) 749-769.

[4] O. Avila-Pozos and A. B. Movchan, Slow decay of end effects in layered structures with an imperfect interface, *Journal of Engineering Mathematics* **45** (2003) 155-168.

[5] Y. Benveniste and T. Miloh, Imperfect soft and stiff interfaces in two-dimensional elasticity, *Mechanics of Materials* **33** (2001) 309-323.

[6] J. R. Berger and A. Karageorghis, The method of fundamental solutions for heat conduction in layered materials. *International Journal for Numerical Methods in Engineering* **45** (1999) 1681-1694.

[7] J. T. Chen and H.-K. Hong, Review of dual boundary element methods with emphasis on hypersingular integrals and divergent series, *ASME Applied Mechanics Reviews* **52** (1999) 17-33.

[8] D. L. Clements, *Boundary Value Problems Governed by Second Order Elliptic Systems*, Pitman, London, 1981.

[9] H. Fan and G. F. Wang, Interaction between a screw dislocation and viscoelastic interfaces, *International Journal of Solids and Structures* **40** (2003) 763-776.

[10] H. Fan and K. Y. Sze, A micro-mechanics model for imperfect interface in dielectric materials, *Mechanics of Materials* **33** (2001) 363-370.

[11] H.-K. Hong and J. T. Chen, Derivations of integral qquations of elasticity, *ASCE Journal of Engineering Mechanics* **114** (1988) 1028-1044

[12] S. Torquato and M. D. Rintoul, Effect of the interface on the properties of composite materials, *Physical Review Letters* **75** (1995) 4067-4070.

[13] Z. Hashin, The spherical inclusion with imperfect interface, *ASME Journal of Applied Mechanics* **58** (1991) 444-449.

Appendix

Consider two dissimilar anisotropic elastic materials occupying the half-spaces $x_2 > 0$ and $x_2 < 0$. The interface $x_2 = 0$ contains periodically distributed line defects defined by

$$p^{(m)} + nL < x_1 < q^{(m)} + nL,\ x_2 = 0\ (m = 1, 2, \cdots, J;\ n = 0, \pm 1, \pm 2, \cdots),$$

where $p^{(m)}$ and $q^{(m)}$ are constants such that $0 < p^{(1)} < q^{(1)} < p^{(2)} < q^{(2)} < \cdots < p^{(M)} < q^{(M)} < L$.

The stress σ_{k2} is continuous on the interface $x_2 = 0$ between the two anisotropic materials, and the displacement u_k is allowed to jump across opposite sides of the line defects but is continuous everywhere else on the interface.

If the bimaterial is subject to an anti-plane deformation governed by (3) with the elastic coefficients given by (2) and if the anti-plane stress σ_{3j} is such that $\sigma_{3j} \to \delta_{j2} S_0$ as $x_1^2 + x_2^2 \to \infty$, then the anti-plane displacement u_3 may be written in the form

$$\begin{aligned} u_3(\xi_1, \xi_2) &= \frac{S_0 \xi_2}{C_{44}(\xi_1, \xi_2)} - \sum_{n=-\infty}^{\infty} \sum_{m=1}^{J} \int_{p^{(m)}+nL}^{q^{(m)}+nL} \Delta u_3(x_1) \\ &\quad \times \left\{ C_{45}^{(1)} \frac{\partial}{\partial x_1} [\Phi(x_1, x_2; \xi_1, \xi_2)] \Big|_{x_2=0^+} \right. \\ &\quad \left. + C_{44}^{(1)} \frac{\partial}{\partial x_2} [\Phi(x_1, x_2; \xi_1, \xi_2)] \Big|_{x_2=0^+} \right\} dx_1 \\ &\quad \text{for } \xi_2 > 0. \end{aligned} \tag{A1}$$

where $\Delta u_3(x_1) = u_3(x_1, 0^+) - u_3(x_1, 0^-)$ denotes the jump of u_3 across the opposite sides of the line defects and $\Phi(x_1, x_2; \xi_1, \xi_2)$ is given by

$$\begin{aligned} \Phi(x_1, x_2; \xi_1, \xi_2) &= \frac{1}{2\pi\beta^{(1)}} \operatorname{Re}\{\ln([x_1 - \xi_1] + \tau^{(1)}[x_2 - \xi_2]) \\ &\quad + \frac{\beta^{(1)} - \beta^{(2)}}{\beta^{(1)} + \beta^{(2)}} \ln(x_1 + \tau^{(1)} x_2 - \xi_1 - \overline{\tau}^{(1)} \xi_2)\} \\ &\quad \text{for } \xi_2 > 0. \end{aligned}$$

with $\beta^{(p)} = \sqrt{|[C_{45}^{(p)}]^2 - C_{44}^{(p)} C_{55}^{(p)}|}$, $\tau^{(p)} = (-C_{45}^{(p)} + i\beta^{(p)})/C_{44}^{(p)}$ and $i = \sqrt{-1}$.

Note that the integral expression in (A1) can be derived from the boundary integral equation for (3) together with the perfect interface Green's function in Berger and Karageorghis [6]. For details on the boundary integral equation, one may refer to Clements [8].

Use of (1) and (A1) together with the periodic property of $\Delta u_3(x_1)$ (that is, $\Delta u_3(x_1) = \Delta u_3(x_1 + L)$) and the formula

$$\sum_{n=1}^{\infty} \frac{1}{(a \pm bn)^2} = \frac{1}{b^2} \psi_1(1 \pm \frac{a}{b}) \text{ for } 1 \pm \frac{a}{b} > 0,$$

yields the interfacial stress formula

$$\begin{aligned} & \sigma_{32}(\xi_1, 0) \\ = \; & S_0 + \frac{\beta^{(1)}\beta^{(2)}}{\pi(\beta^{(1)} + \beta^{(2)})} \sum_{m=1}^{J} \oint\!\!\!\!\!\!= _{p^{(m)}}^{q^{(m)}} \Delta u_3(x_1) [\frac{1}{(x_1 - \xi_1)^2} + \frac{1}{(L + x_1 - \xi_1)^2} \\ & + \frac{1}{(L + \xi_1 - x_1)^2} + \frac{1}{L^2} \psi^*(\frac{L + x_1 - \xi_1}{L}) + \frac{1}{L^2} \psi^*(\frac{L + \xi_1 - x_1}{L})] dx_1 \\ & \text{for } p^{(n)} < \xi_1 < q^{(n)} \; (n = 1, 2, \cdots, J), \end{aligned} \tag{A2}$$

where $\oint\!\!\!\!\!\!=$ denotes that the integral is to be interpreted in the Hadamard finite-part sense, $\psi^*(x) = \psi_1(x) - 1/x^2$ and $\psi_1(x)$ is the trigamma function defined by

$$\psi_1(x) = \int_0^{\infty} \frac{t \exp(-xt) dt}{1 - \exp(-t)}.$$

Note that the function $\psi^*(x)$ tends to $\pi^2/6$ as $x \to 0^+$. In fact, it can be shown that $0 < \psi^*(x) < \pi^2/6$ for $x > 0$. Accurate and efficient algorithms for evaluating $\psi^*(x)$ are available (Abramowitz and Stegun [1]).